Supporting information

Dual-Functional $CF_3SO_3^-$/Amine Additives Synergistically Construct MgF_2/Mg_3N_2-Rich Interphase toward High-Performance Magnesium-Sulfur Batteries

Jiaming Shi[a,†], Miao Cheng[a,†,*], Qianqian Liu[a], Ruirui Wang[a], Wujun Ma[b], Jing Hu[a], Tao Wei[a], Bo Liu[a,*], Muzi Chen[c], Wanfei Li[a,*]

[a] *Suzhou Key Laboratory for Nanophotonic and Nanoelectronic Materials and Its Devices, School of Materials Science and Engineering, Suzhou University of Science and Technology, Suzhou 215009, Jiangsu Province, China*

[b] *College of Textile and Garment, Nantong University, Nantong, 226019, Jiangsu Province, China*

[c] *Soochow Univ, Anal & Testing Ctr, Suzhou 215123, Jiangsu Province, China*

[†] *Both authors contributed equally to this work*

[*] *Corresponding authors.*

E-mail address: chengmiao@usts.edu.cn (Miao Cheng), wfli2018@mail.usts.edu.cn (Wanfei Li), liubo@mail.usts.edu.cn (Bo Liu)

Computational methodology

Molecular dynamics simulated annealing was performed using Gromacs 2024.2 [S1, S2] software to explore low-energy conformations of three-molecule clusters. Atomic partial charges were assigned via the restrained electrostatic potential (RESP) method implemented in Multiwfn 3.8(dev) [S3, S4]. Ten annealing cycles were conducted with temperatures ramped from 0 to 400 K. Then, the lowest-energy configuration from annealing underwent structural optimization and frequency analysis at the PBE0[S5]-D3(BJ) [S6, S7]/6-311G** [S8, S9] theory level using Gaussian 16 A.03 [S10]. All geometry optimizations employed the polarizable continuum model (PCM) [S11] with a solvent dielectric constant of $\varepsilon = 9.6$, determined from the volumetric ratio (1:1) of DME to PYR14TFSI. Binding energies (ΔE) were computed at the higher PBE0-D3(BJ)/ma-def2-TZVP [S12-S14] level according to:

$$\Delta E = E(\text{complex}) - \Sigma E(\text{monomers})$$

Frontier molecular orbital energies (HOMO/LUMO) were derived from optimized structures. Wavefunction analyses were conducted with Multiwfn 3.8(dev) [S3, S4], and molecular visualizations were generated using VMD 1.9.3 [S15] software.

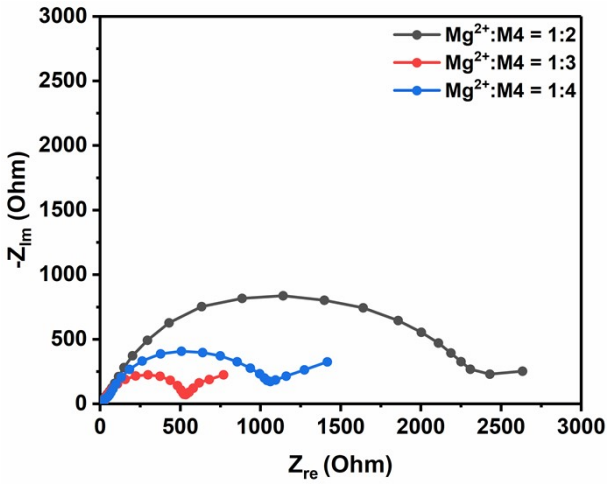

Figure S1 Nyquist plots of the Mg||Mg symmetrical cells with varying Mg^{2+}:M4 molar ratios in MAID-NaOTf-M4 electrolyte.

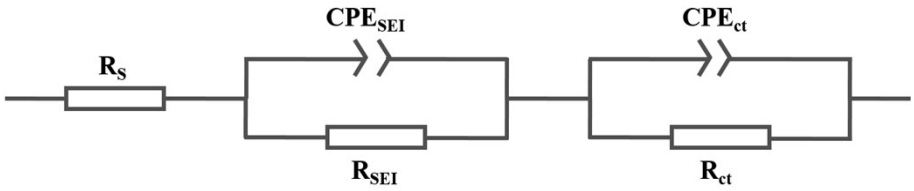

Figure S2 Equivalent circuit model for fitting Nyquist plots.

Table S1 EIS fitting results for Mg||Mg symmetrical cells after standing in MAID, MAID-NaOTf, MAID-M4 and MAID-NaOTf-M4 electrolyte.

Electrolyte		0 h	1 h	2 h	3 h
MAID	R_s (Ω)	2.9	2.9	3.0	3.0
	R_{SEI} (Ω)	45.7	58.2	150.1	164.2
	R_{ct} (Ω)	7392.8	7840.1	11726.0	13493.0
MAID-NaOTf	R_S (Ω)	3.5	3.6	3.7	3.8
	R_{SEI} (Ω)	59.2	142.3	330.9	351.3
	R_{ct} (Ω)	9162.1	13995.0	18094.0	22463.2
MAID-M4	R_s (Ω)	3.5	3.7	4.0	4.1
	R_{SEI} (Ω)	80.6	97.7	122.1	122.4
	R_{ct} (Ω)	3795.2	6909.3	8165.0	8401.0
MAID-NaOTf-M4	R_s (Ω)	4.0	4.6	5.3	5.8
	R_{SEI} (Ω)	19.0	14.3	16.2	15.5
	R_{ct} (Ω)	530.5	422.3	487.4	581.8

Table S2 EIS fitting results for Mg||Mg symmetrical cells with varying Mg^{2+}:M4 molar ratios in MAID-NaOTf-M4 electrolyte.

Mg^{2+}:M4 (Molar ratio)	1:2	1:3	1:4
R_s (Ω)	3.5	4.0	5.4
R_{SEI} (Ω)	27.1	19.0	29.6
R_{ct} (Ω)	2281.9	530.5	1140.1

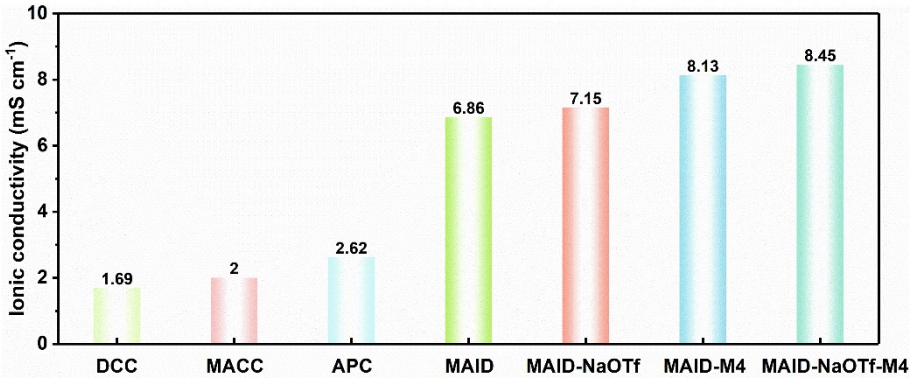

Figure S3 Ionic conductivity of the electrolytes.

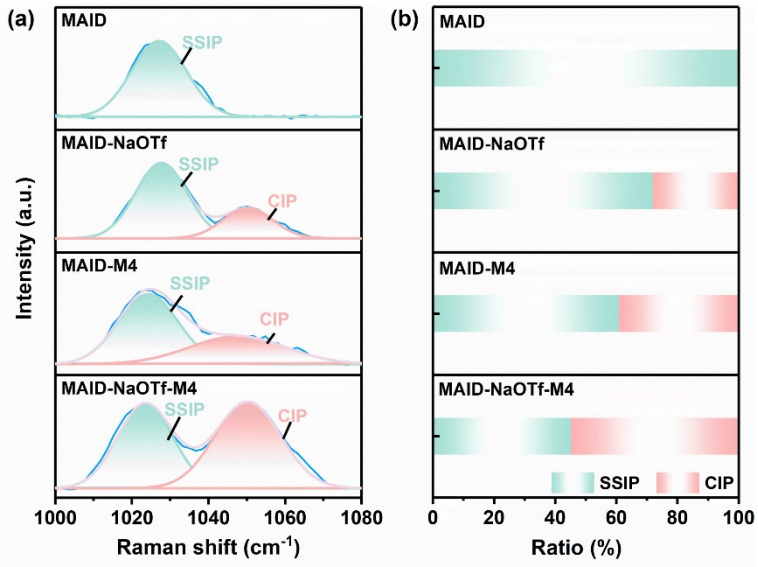

Figure S4 Raman spectra of the four electrolytes (a) and the change in the proportion of SSIP and CIP (b).

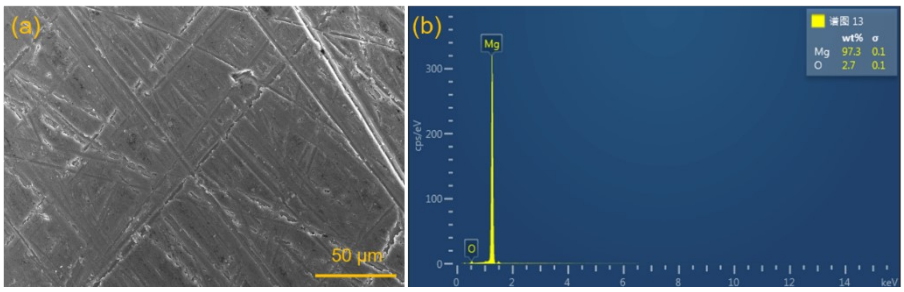

Figure S5 SEM image of the polished Mg anode (a) and corresponding elemental content (b).

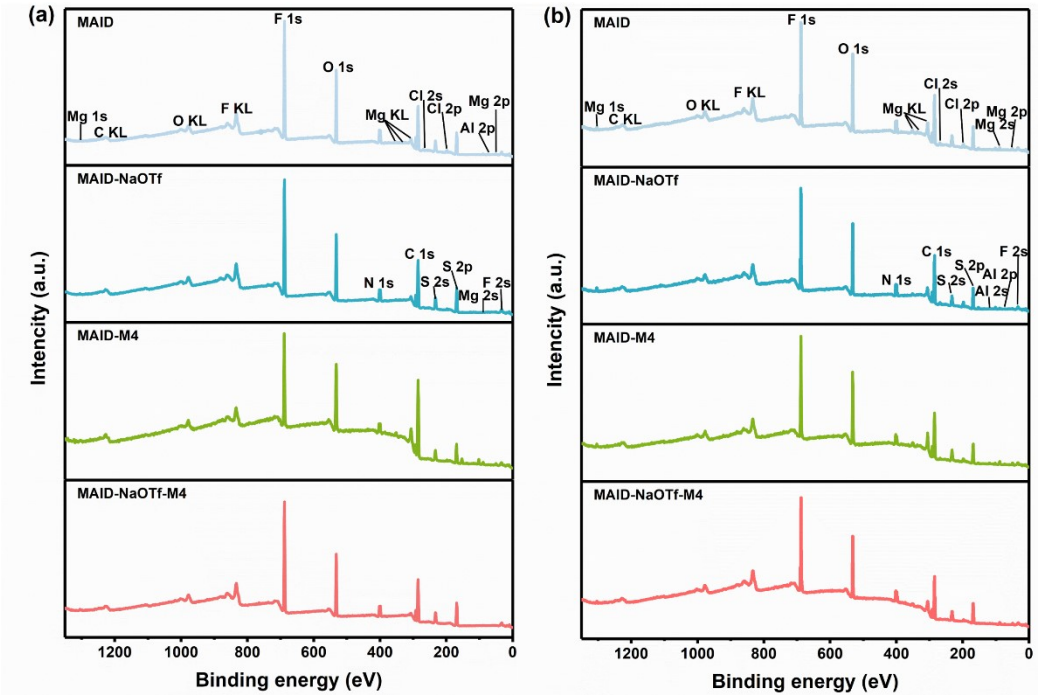

Figure S6 The XPS survey of the Mg anode surface after 1 hour standing with the four electrolytes (a); the XPS survey of the Mg anode surface in Mg||Mg cells after 1 hour standing and cycling for 50 cycles with these electrolytes (b).

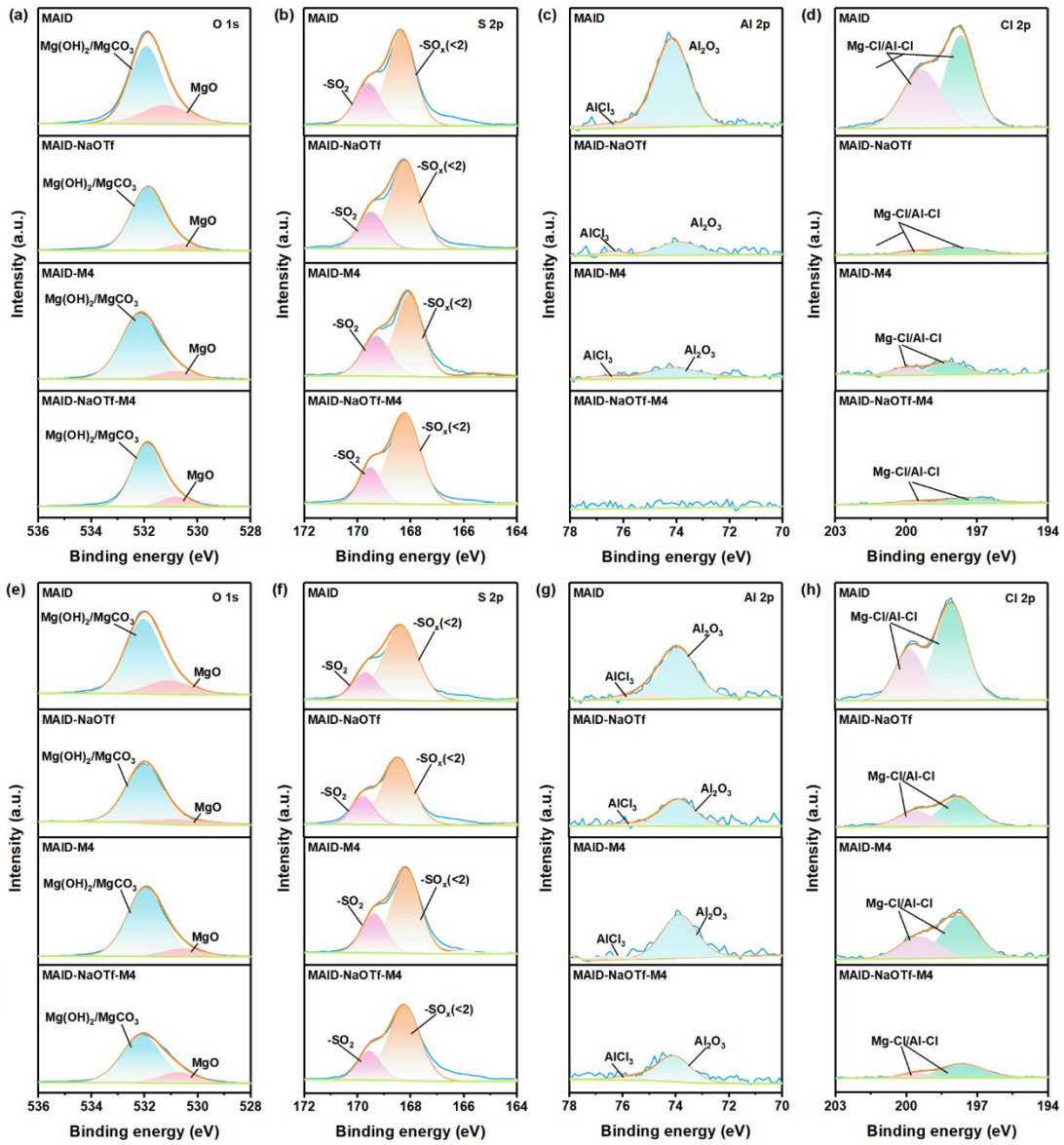

Figure S7 O 1s (a), S 2p (b), Al 2p (c) and Cl 2p (d) XPS spectra of Mg anode surface after 1 hour standing in these electrolytes; O 1s (e), S 2p (f), Al 2p (g) and Cl 2p (h) XPS spectra of Mg anode surface in Mg||Mg cells after 1 hour standing and cycling for 50 cycles with these electrolytes.

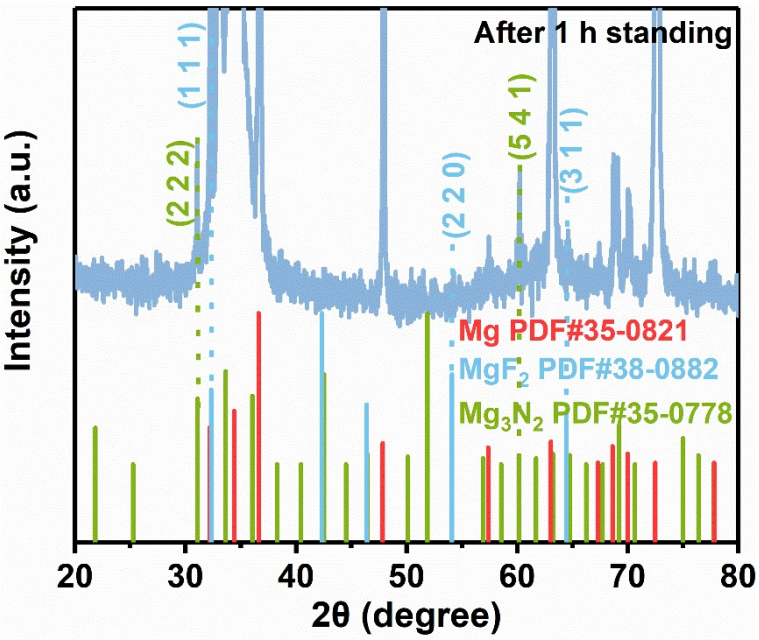

Figure S8 XRD pattern of the Mg anode after 1 hour standing in MAID-NaOTf-M4 electrolyte.

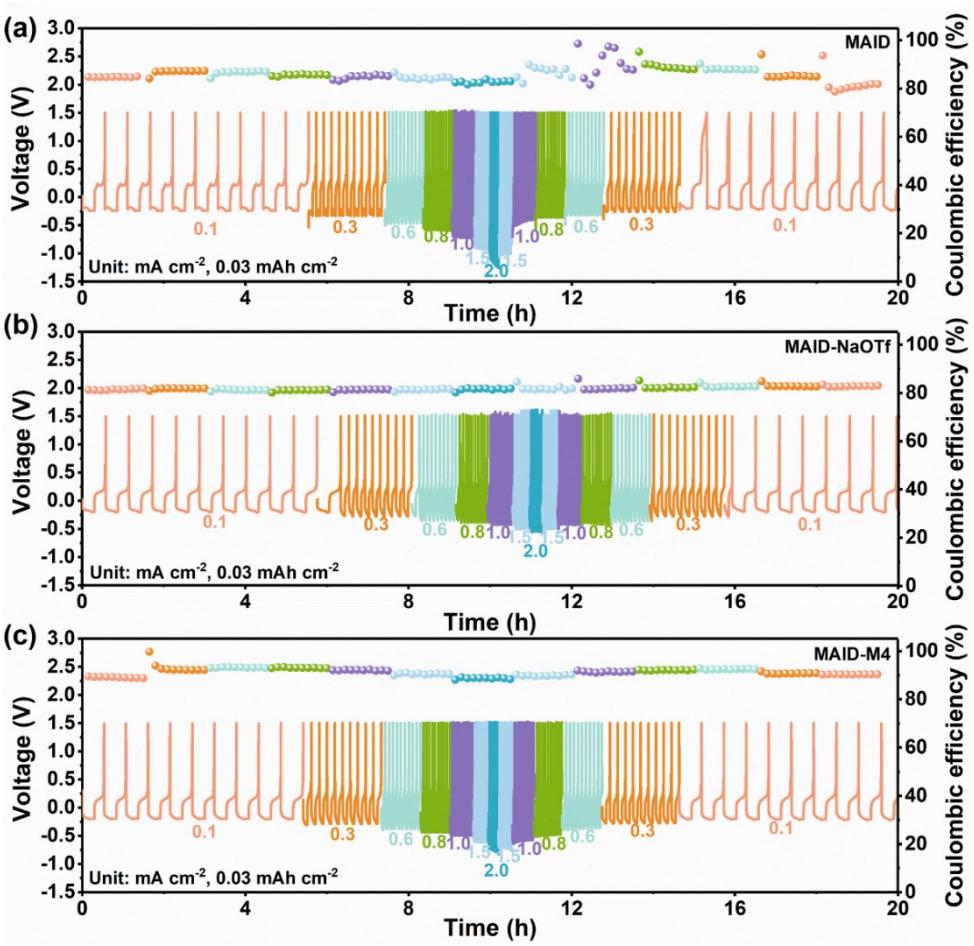

Figure S9 The plating/stripping profiles and CEs of Mg||Cu cells with MAID (a) MAID-NaOTf (b) and MAID-M4 (c) electrolytes with varied current densities (0.1-2.0 mA cm^{-2} with 0.03 mAh cm^{-2}).

Table S3 The rate performance of Mg||Cu cells with different electrolytes.

Electrolyte	MAID	MAID-NaOTf	MAID-M4	MAID-NaOTf-M4
Current density ($mA\ cm^{-2}$)	Discharge overpotential (V)			
0.1	0.19	0.19	0.18	0.16
0.3	0.22	0.22	0.22	0.19
0.6	0.28	0.29	0.27	0.20
0.8	0.31	0.32	0.32	0.23
1.0	0.35	0.37	0.36	0.25
1.5	0.43	0.49	0.48	0.29
2.0	0.75	0.76	0.65	0.33

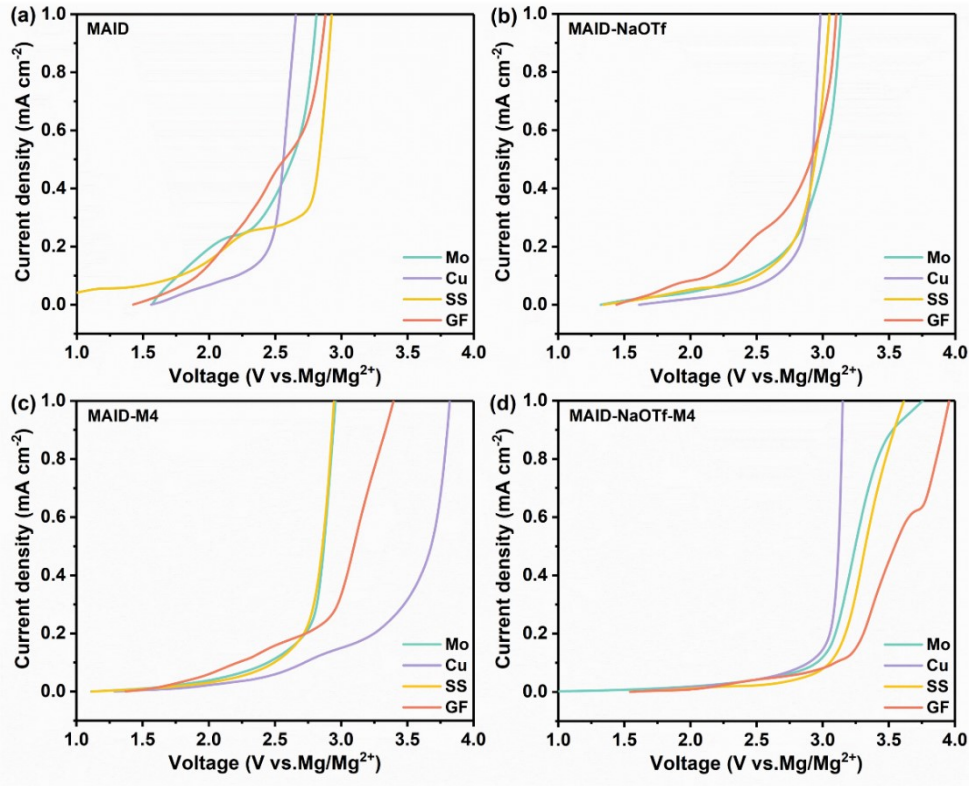

Figure S10 LSV curves of MAID (a), MAID-NaOTf (b), MAID-M4 (c) and MAID-NaOTf-M4 (d) on different working electrodes (Mo, Cu, SS and GF).

Table S4 The oxidation stability of the four electrolytes on different working electrodes (V).

Electrolyte	Pt	Mo	Cu	SS	GF
MAID	3.0	1.8	2.2	1.8	1.9
MAID-NaOTf	3.2	2.4	2.6	2.5	2.1
MAID-M4	3.1	2.4	2.7	2.5	2.2
MAID-NaOTf-M4	3.4	3.0	2.9	3.1	3.1

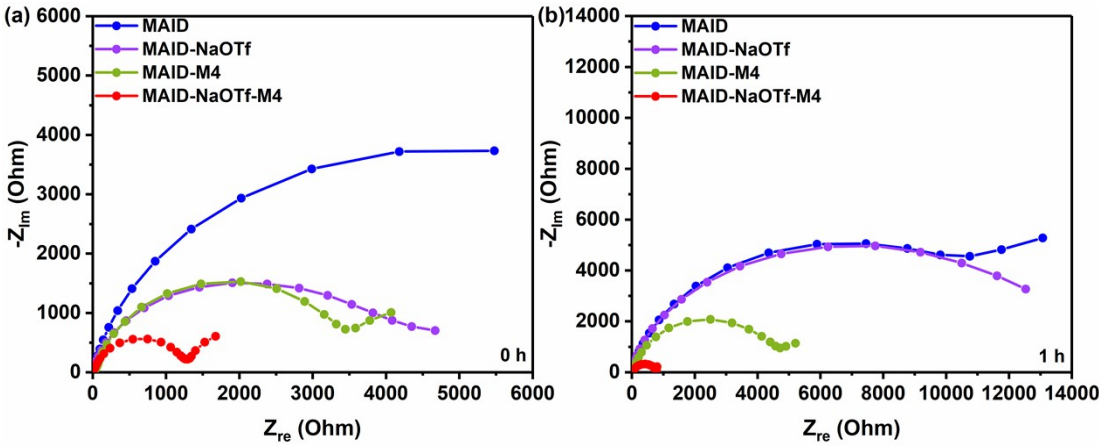

Figure S11 Nyquist plots of Mg||CMK-3@$S_{0.86}Se_{0.14}$ cells with four electrolytes after 0 h (a) and 1 h (b) standing.

Table S5 EIS fitting results of the Mg||CMK-3@$S_{0.86}Se_{0.14}$ cells with four electrolytes after standing for 0 and 1 h.

Electrolyte	Time	R_s (Ω)	R_{SEI} (Ω)	R_{ct} (Ω)
MAID	0 h	2.7	338.4	8895.9
	1 h	2.9	2106.1	11064.0
MAID-NaOTf	0 h	2.9	668.9	5371.0
	1 h	3.5	2873.0	11695.0
MAID-M4	0 h	3.7	241.3	3672.0
	1 h	4.1	493.2	4873.0
MAID-NaOTf-M4	0 h	5.1	84.7	1226.4
	1 h	6.1	27.3	766.5

Table S6 Comparison of the electrochemical performance of Mg/S batteries using MAID-NaOTf-M4 and state-of-the-art electrolytes.

Electrolyte	Sulfur cathode	Current collector	Specific capacity (mAh g^{-1})	Reversible capacity (mAh g^{-1})	Cycle numbers	Ref.
THFPE-MgF_2-DME	S_8@NdMC	Al@C	660 (0.02 C)	400 (0.05 C)	20	S16
$Mg(TFSI)_2$-TBABr+BTT	CNT@KB/S	Al@C	800 (0.1 C)	468 (0.1 C)	30	S17
$Mg(HMDS)_2$-$AlCl_3$-DOL/DME	CNTS	Al@C	654 (0.05 C)	270 (0.2 C)	100	S18
$Mg[B(hfip)_4]_2$/DME	S/CMK-3	Al@C	449 (0.1 C)	152 (0.5 C)	500	S19
$Mg[B(hfip)_4]_2$/G1	CMC-SBR/KB/S/	Al@C	650 (0.05 C)	69 (0.1 C)	150	S20
$Mg[B(hfip)_4]_2$·3DME	KB/S	Al@C	468 (0.1 C)	320 (0.1 C)	100	S21
$Mg(TFSI)_2$-DME-M4	KB/S	Al	485.2 (0.1 C)	312.2 (0.1 C)	30	S22
MgBOR−PTHF−GPE	ACC/S	Activated carbon cloth	741 (0.1 C)	500 (0.1 C)	20	S23
$BMIMBF_4$-$Mg(TFSI)_2$	S@CNTS	SS	386 (300 mA g^{-1})	334 (300 mA g^{-1})	100	S24
MBA-$(MgCl_2)_2$ $(AlCl_3)_2$+LiCl/THF	S@pPAN	Cu/SS	1050 (0.05 C)	515 (0.1 C)	85	S25

$MgCl_2$-LiCl/THF	STAR@ LCNC-S	Cu@C	925 (0.1 C)	577 (0.5 C)	400	S26
$[Mg·6THF][AlCl_4]_2$-LiCl	NG-NCNT@NCS @S	Cu	869 (0.1 C)	300 (0.4 C)	500	S27
$AlCl_3$-$InCl_3$/TEG	KB/S	Cu	1150 (0.01 C)	800 (0.05 C)	50	S28
PMC	$Mo_{0.075}V_{0.925}Se_2$/S	Cu	1021 (100 mA g^{-1})	835 (1 A g^{-1})	200	S29
$Mg(CF_3SO_3)_2$-$MgCl_2$-$AlCl_3$-$LiCF_3SO_3$	Cu/Ni-NiO/C-S	Cu	1290 (0.1 A g^{-1})	914 (0.2 A g^{-1})	200	S30
MAID-NaOTf-M4	CMK-3 @$S_{0.86}Se_{0.14}$	Cu	1142.2 (0.05 C)	675.2 (0.1 C)	200	This work

References

[S1] M. J. Abraham T. Murtola, R. Schulz, S. Páll, J. C. Smith, B. Hess and E. Lindahl, *SoftwareX*, 2015, **1**, 19-25.

[S2] S. Pronk, S. Páll, R. Schulz, P. Larsson, P. Bjelkmar, R. Apostolov, M. R. Shirts, J. C. Smith, P. M. Kasson, D. Spoel, B. Hess and E. Lindahl, *Bioinformatics*, 2013, **29**, 845-854.

[S3] T. Lu and F. Chen, *J. Comput. Chem.*, 2012, **33**, 580-592.

[S4] T. Lu, *J. Chem. Phys.*, 2024, **161**, 082503.

[S5] C. Adamo and V. Barone, *J. Chem. Phys.*, 1999, **110**, 6158-6170.

[S6] S. Grimme, *WIREs Comput. Mol. Sci.*, 2011, **1**, 211-228.

[S7] S. Grimme, S. Ehrlich and L. Goerigk, *J. Comput. Chem.*, 2011, **32**, 1456-1465.

[S8] P. C. Hariharan and J. A. Pople, *Theor. Chim. Acta*, 1973, **28**, 213-222.

[S9] W. J. Hehre, R. Ditchfield and J. A. Pople, *J. Chem. Phys.*, 1972, **56**, 2257-2261.

[S10] M. J. Frisch, G. W. Trucks, H. B. Schlegel, G. E. Scuseria, M. A. Robb, J. R. Cheeseman, G. Scalmani, V. Barone, G. A. Petersson, H. Nakatsuji, X. Li, M. Caricato, A. V. Marenich, J. Bloino, B. G. Janesko, R. Gomperts, B. Mennucci, H. P. Hratchian, J. V. Ortiz, A. F. Izmaylov, J. L. Sonnenberg, Williams, F. Ding, F. Lipparini, F. Egidi, J. Goings, B. Peng, A. Petrone, T. Henderson, D. Ranasinghe, V. G. Zakrzewski, J. Gao, N. Rega, G. Zheng, W. Liang, M. Hada, M. Ehara, K. Toyota, R. Fukuda, J. Hasegawa, M. Ishida, T. Nakajima, Y. Honda, O. Kitao, H. Nakai, T. Vreven, K. Throssell, Jr. J. A. Montgomery, J. E. Peralta, F. Ogliaro, M. J. Bearpark, J. J. Heyd, E. N. Brothers, K. N. Kudin, V. N. Staroverov, T. A. Keith, R. Kobayashi, J. Normand,

K. Raghavachari, A. P. Rendell, J. C. Burant, S. S. Iyengar, J. Tomasi, M. Cossi, J. M. Millam, M. Klene, C. Adamo, R. Cammi, J W. Ochterski, R. L. Martin, K. Morokuma, O. Farkas, J. B. Foresman and D. J. Fox, *Gaussian 16 rev. A.03.*, 2016.

[S11] S. Miertus, E. Scrocco and J. Tomasi, *Chem. Phys.*, 1981, **55**, 117-129.

[S12] F. Weigend and R. Ahlrichs, *Phys. Chem. Chem. Phys.*, 2005, **7**, 3297-3305.

[S13] F. Weigend, *Phys. Chem. Chem. Phys.*, 2006, **8**, 1057-1065.

[S14] J. Zheng, X. Xu and D. G. Truhlar, *Theor. Chem. Acc.*, 2011, **128**, 295-305.

[S15] W. Humphrey, A. Dalke and K. Schulten, *J. Mol. Graph. Model.*, 1996, **14**, 33-38.

[S16] M. Lee, M. Jeong, Y. S. Nam, J. Moon, M. Lee, H. D. Lim, D. Byun, T. Yim and S. H. Oh, *J. Power Sources*, 2022, **535**, 231471.

[S17] Q. Lin, J. Xiao, Z. S. Ng, X. Zhang, W. Chen, T. Wang, J. Hu, Y, Su and Y. Zhang, *Adv. Funct. Mater.*, 2025, **35**, 2506192.

[S18] R. K. Bhardwaj and A. J. Bhattacharyya, *ACS Appl. Energy Mater.*, 2021, **4**, 14121-14128.

[S19] Y. Yang, W. Fu, D. Zhang, W. Ren, S. Zhang, Y. Yan, Y. Zhang, S. J. Lee, J. S. Lee, Z. F. Ma, J. Yang, J. Wang and Y. NuLi, *ACS Nano*, 2023, **17**, 1255-1267.

[S20] J. Häcker, T. Rommel, P. Lange, Z. Zhao-Karger, T. Morawietz, I. Biswas, N. Wagner, M. Nojabaee and K. A. Friedrich, *ACS Appl. Mater. Interfaces*, 2023, **15**, 33013-33027.

[S21] Y. Ji, X. Liu-Théato, Y. Xiu, S. Indris, C. Njel, J. Maibach, H. Ehrenberg, M. Fichtner and Z. Zhao-Karger, *Adv. Funct. Mater.*, 2021, **31**, 2100868.

[S22] C. Wei, L. Tan, Y. Zhang, B. Xi, S. Xiong, J. Feng and Y. Qian, *Energy Storage Mater.*, 2022, **48**, 447-457.

[S23] L. Wang, Z. Li, Z. Meng, Y. Xiu, B. Dasari, Z. Zhao-Karger and M. Fichtner, *Energy Storage Mater.*, 2022, **48**, 155-163.

[S24] S. Rayamma, J. V. Rani and L. Malyala, *Rasayan J. Chem.*, 2025, **18**, 2433-2443.

[S25] S. Zhang, W. Ren, Y. NuLi, B. Wang, J. Yang and J. Wang, *Chem. Eng. J.*, 2022, **427**, 130902.

[S26] Q. Guan, J. Wang, Q. Zhuang, J. Zhang, L. Li, L. Jia, Y. Zhang, H. Hu, H. Hu, S. Cheng, H. Zhang, H. Li, M. Liu, S. Wang and H. Lin, *Energy Environ Sci.*, 2024, **17**, 3765-3775.

[S27] H. Fan, Z. Zheng, L. Zhao, W. Li, J. Wang, M. Dai, Y. Zhao, J. Xiao, G. Wang, X. Ding, H. Xiao, J. Li, Y. Wu and Y. Zhang, *Adv. Funct. Mater.*, 2020, **30**, 1909370.

[S28] R. Li, R. Zhang, Q. Liu, J. An, Y. Song, B. Deng, Y. Ma, H. Huo, Y. Gao, J. Wang, P. Zuo and G. Yin, *Chem. Eng. J.*, 2023, **462**, 141998.

[S29] R. Jiang, M. Jin, C. Du, T. Song, X. Ma, Y. Zhu, C. Cao and M. Zou, *Adv. Energy Mater.*, 2026, **16**, e05028.

[S30] Y. Sun, H. Cui, X. Yan, X. Zhang, X. Zhao, Z. Kou, B. Liu and Z. Cheng, *J. Alloy. Compd.*, 2025, **1026**, 180551.